

# **Improving phased array ultrasonic testing using models to overcome austenitic weld distortion**

C. Nageswaran, C. Carpentier, TWI Ltd, UK; Y.Y. Tse, Birmingham University, UK

## **ABSTRACT**

The fundamental obstacle to accurately characterising the defects in austenitic welds is the distortion of the sound field due to the anisotropic inhomogeneous material. This paper describes the development of the next generation of ultrasonic procedures which use phased array techniques and models to account for the distortion of the sound field, such that the detection, positioning and sizing of defects is improved in comparison to current capabilities.

Each stage of the procedure development is described along with the issues and obstacles which must be overcome. Electron Back Scatter Diffraction (EBSD) techniques are used to evaluate the texture of the weld and then the microstructural information is input to a model capable of propagating ultrasonic waves through the anisotropic inhomogeneous medium. With knowledge of the distortion, two routes are investigated for improving inspection: (1) adapting focal laws to correctly position and size the discontinuities and (2) applying corrections to detected signals using the scanning procedure. This paper presents the results from the ongoing project funded by the UK Technology Strategy Board ([www.dissimilarweld.co.uk](http://www.dissimilarweld.co.uk)).

## **INTRODUCTION**

The difficulties associated with the ultrasonic non-destructive evaluation of austenitic welds are well known. The fundamental issue is the distortion of a propagating elastic stress wave (ie sound) by the coarse-grained anisotropic weld metal. The large grains tend to scatter the sound energy leading to increased attenuation and the propagation path is 'skewed' due to the anisotropy of the crystal structure and the differences in texture between different regions in the weld. Consequently, the noise due to grain backscattering reduces the sensitivity (ie signal-to-noise (S/N) performance) and the sound beam skewing leads to incorrect interpretation of flaws - ie positioning and sizing errors. Additionally, the weld metal condition can conspire to generate spurious indications which could be erroneously interpreted as defects that threaten structural integrity [1].

In recent times, the development and increasing maturity of three fields have opened the possibility of overcoming the difficulties of inspecting austenitic welds, such that the next generation of ultrasonic procedures can inspect the welds in critical components with reduced errors and greater confidence. Namely the three fields are: (1) microstructural quantification, (2) models and (3) array ultrasonic technology.

The ongoing project (termed DISSIMILAR) is an attempt to draw together the advanced tools from within these three fields to generate novel ultrasonic inspection procedures tailored to austenitic welds. This paper presents results to date, illustrating the methods used to quantify the microstructure, modelling results and the proposed strategies to overcome the distortion of the sound field by the material.

## **BACKGROUND**

A previous European Union funded Framework VI project (RIMINI) was used to develop an immersion coupled phased array probe to improve the S/N performance when inspecting thick-sectioned dissimilar welds in the nuclear power plant [2]. The RIMINI project showed that adapting the concept of separating the transmit and receive paths to an array probe, using longitudinal waves and a two-dimensional matrix led to improvements in the achieved S/N, when compared to best practice conventional twin-crystal probes. The RIMINI probe is used below to illustrate the errors induced by the distortion of the sound field.

Figure 1 shows a dissimilar weld specimen representative of the surge-end nozzle weld from a modern pressurised water nuclear power plant. The weld was made of Inconel 182 which was

deposited on a ferritic parent that was clad (using 309L/308L) and buttered with a 5mm layer of Inconel 182.

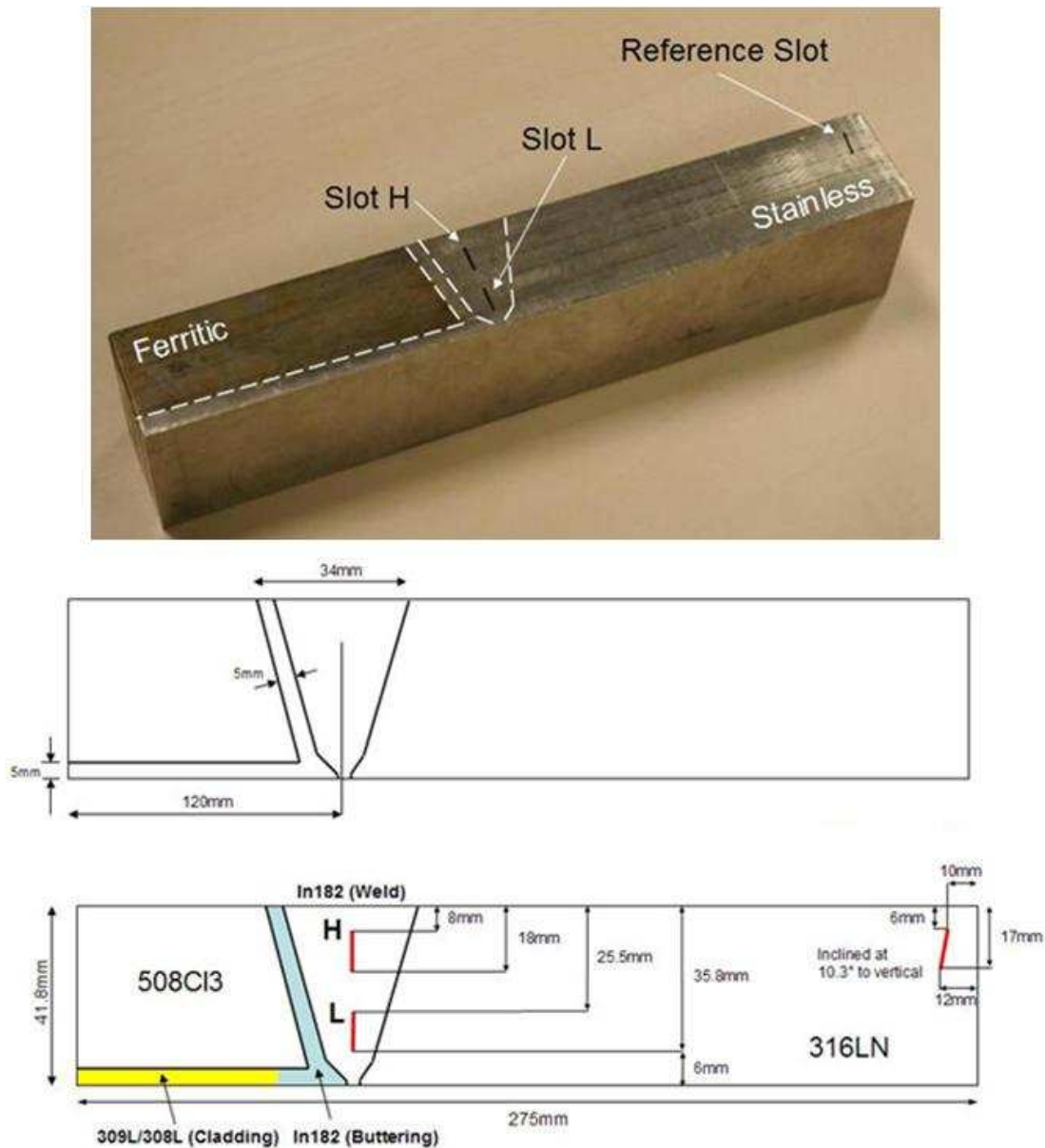
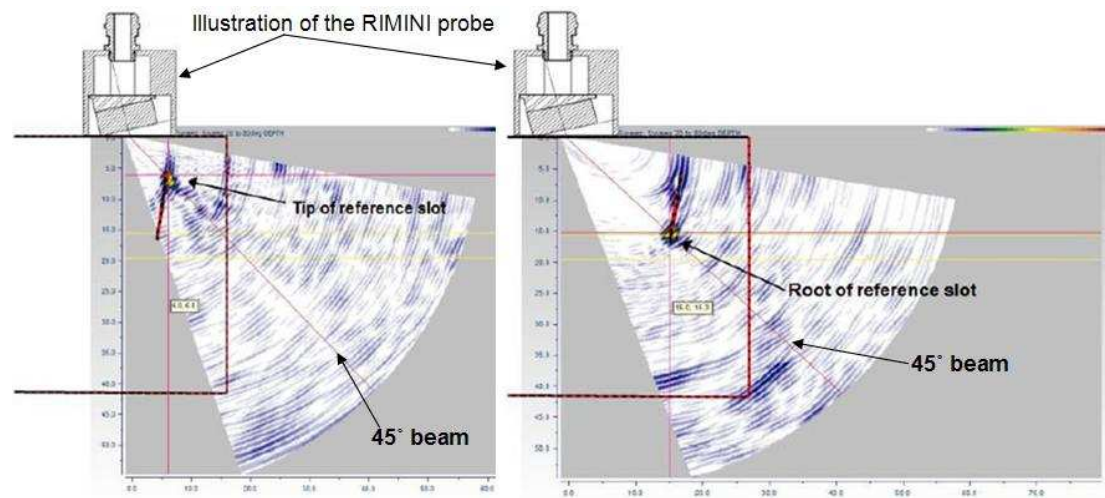


**Figure 1** A representative test specimen of the surge-end nozzle dissimilar weld, with two vertical slots implanted on the centerline of the weld and an inclined reference slot implanted in the parent stainless steel.

Figure 2 illustrates the calibration on the reference slot embedded within the parent stainless steel. Note the terminology, where the diffraction signal from the top of the slot is termed the ‘tip’ signal and that from the bottom of the slot is termed the ‘root’ signal. The calibration S/N performance of the probe was greater than 20dB when putting the diffraction signals at 80% full screen height (FSH).

Note that in all the data shown in Figures 2, 3 and 4 the probe was programmed to focus the sound at the depth of the tip/root of the slot under interrogation, with the resultant signal shown plotted along the 45° beam. Hence, in Figure 2, the left image shows the signal along the 45° beam (the red line) when the sound was focused to the tip depth of the reference slot and right image shows the data along the 45° beam when the sound was focused to the root depth. To place the relevant signal along the 45° beam line, the probe was moved on the surface of the specimen. The weld overlay and the

positions of the probe are dimensionally accurate, and are used to illustrate the distorting effects of the weld in Figures 3 and 4.



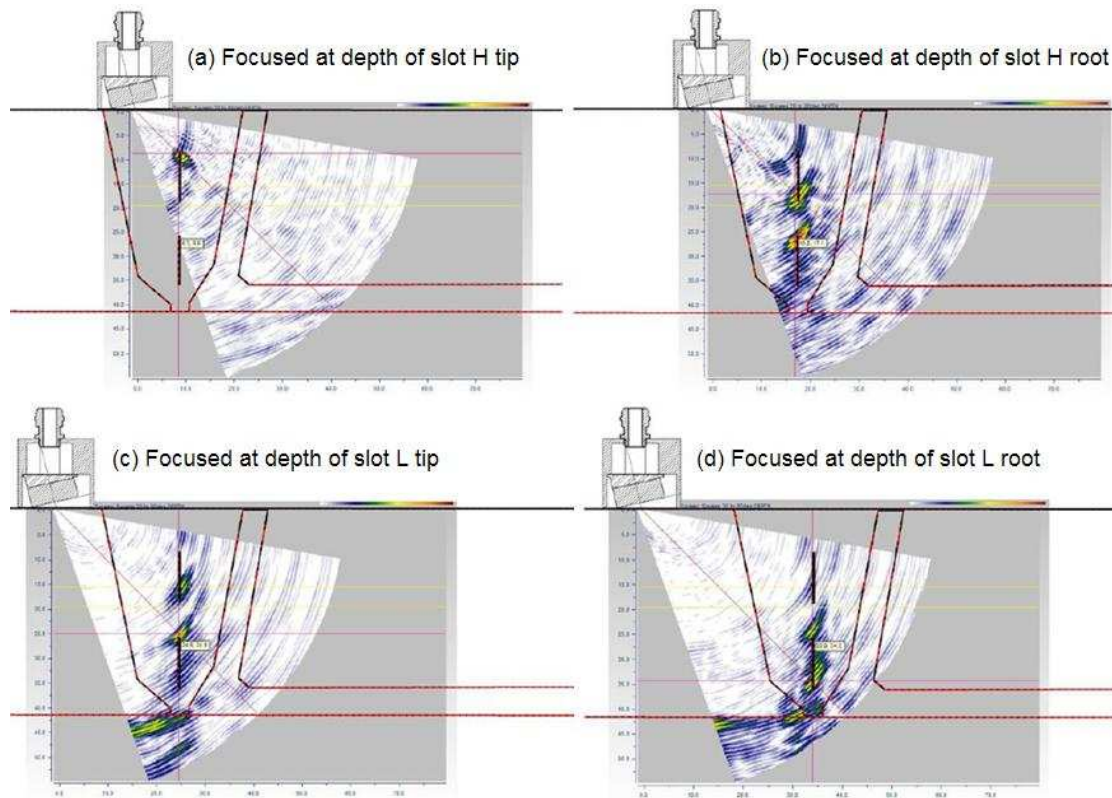
**Figure 2** Calibration of the RIMINI probe on the reference slot using the diffracted signals from the tip and root of the slot placed at 80% FSH.

Figure 3 shows the data for inspection of the two slots H and L with the probe placed on the parent stainless steel, ie approaching the slots through the weld-stainless interface. To place the tip signal of slot H at 80% FSH the system gain was increased by 12dB from calibration, illustrating the degree of attenuation within the weld (see Figure 3(a)). Note that the tip of slot H was 8mm below the top surface, illustrating the good near-surface performance of the RIMINI probe [2]; additionally, the S/N performance of the probe in Figure 3(a) was greater than 20dB.

Figure 3(b) shows the probe focused at a depth corresponding to the root of slot H, with the signal due to the root plotted along the 45° beam line. Firstly, the system gain increase required to place the slot H root signal at 80% FSH was 22.75dB above calibration, implying rapidly increasing attenuation. Secondly, note the distortion of the sound field near the tip of slot H giving rise to two indications in the vicinity. Thirdly, the actual maximum energy of the sound field is skewed to the position of the tip of slot L, rather than root of slot H, as evident from the greater signal amplitude of the diffracted signal from the tip of slot L.

Figure 3(c) shows the probe focusing at the tip of slot L and the resultant tip signal plotted along the 45° beam line. Note that the sound field energy maximum is in the vicinity of the tip of slot L, as was the case when focusing instead to the root of slot H as shown in Figure 3(b). Hence it appears that the local microstructure, or specifically the actual sound path, has a significant influence on the distribution of the sound energy. In addition, note that the error in positioning of the diffraction signal due to the root of slot H, with respect to the tip of slot L, is greater than 2mm. Similar positioning errors are evident when focusing to the root of slot L, where the tip of slot L plots incorrectly, in addition to spurious signals probably due to the body of slot L (see Figure 3(d)).

In summary, the microstructure of the weld distorts the propagating sound energy to such a degree that significant inaccuracies in positioning and sizing are induced, reducing confidence in the interpretation of the inspection results.



**Figure 3** Inspection of the slots embedded in the weld with the RIMINI probe placed on the parent stainless steel, with the sound propagating into the weld along the weld-stainless interface.

In the case of dissimilar welds, the use of cladding and buttering lead to further complications, as illustrated in Figure 4. In this case, the RIMINI probe was placed on the parent ferritic for the inspection of the two slots embedded in the weld, with the sound propagating through the Inconel 182 buttering. The probe was programmed to focus the sound to the depth of slot L root; however the sound energy maximum is strongly skewed upwards towards the tip of slot L. Additionally, note the significant backscattered signal from the cladding which leads to difficulties for resolving signals emanating from flaws at the root of the weld. The use of clad line pipes is increasing for the transport of corrosive petrochemical commodities; consequently, the need to improve confidence in the inspection of such line pipes, where flaws in the weld root are critical, is greater.

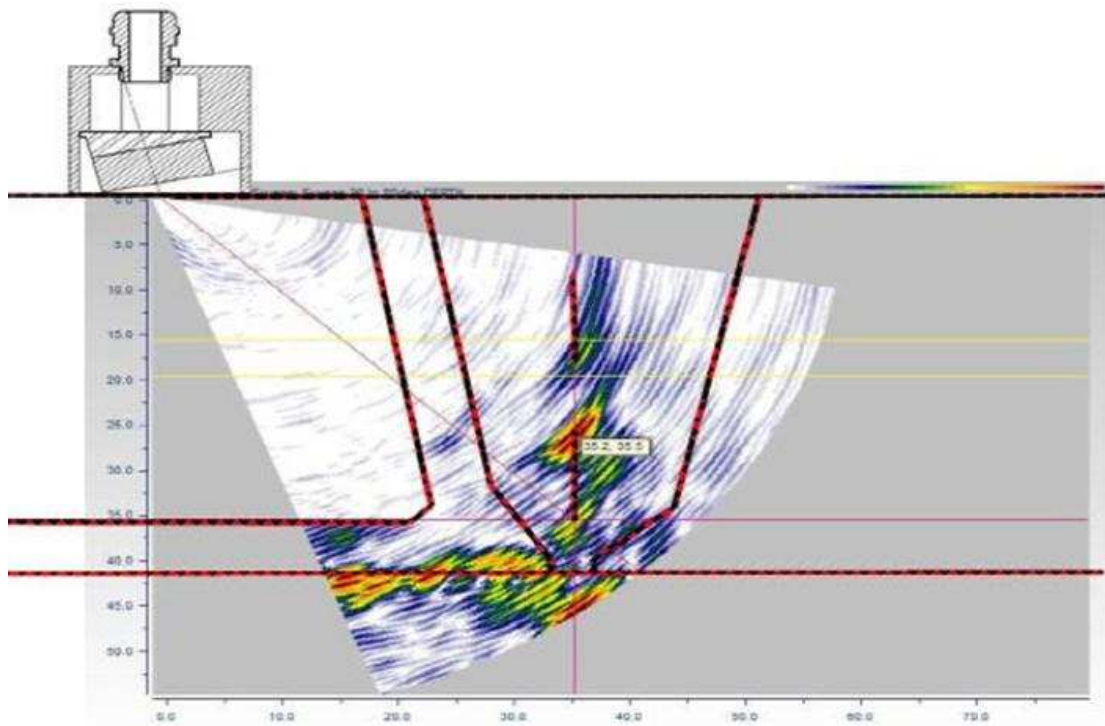


**Figure 4** Inspection of the slots embedded in the weld with the RIMINI probe placed on the parent ferritic steel, with the sound propagating into the weld through the buttering; the probe was programmed to focus at the depth of slot L root.

Significant effort is underway around the world to make use of phased array technology to address the issues of inspecting austenitic welds [3, 4, and 5]. A major aspect of the DISSIMILAR project is to follow the successful development of the RIMINI probe through further exploration of transmit-receive longitudinal (TRL) designs, as well as investigate the use of innovative segmented matrix array annular designs. The emphasis in the DISSIMILAR project is the improvement of transducer technology through the use of single-crystal piezocomposite materials and optimisation of bandwidth/sensitivity performance.

Ultimately, however, the transducer cannot overcome the distortion imparted onto the propagating sound wave by the coarse-grained anisotropic weld. To improve inspection quality, the material condition has to be taken into account at the inspection design stage and during data interpretation.

## APPROACH

### Microstructural quantification

To design the inspection with due consideration to the complex material through which the ultrasound has to propagate, the material must be quantified. In the case of the coarse-grained anisotropic austenitic metals, the description must (1) identify the grain boundaries and (2) evaluate the texture developed in the weld. Furthermore, to evaluate the implications to sound propagation, the elastic stiffness encountered by a wave must be known.

The electron back scattered diffraction (EBSD) technique in a scanning electron microscope is widely used to determine the microtexture of crystalline materials [6]. An electron beam is incident on a specimen tilted at  $70^\circ$  to the horizontal to allow more electrons to undergo diffraction and escape the sample surface. The austenitic weld surface was mechanically polished with Silica colloidal as final finishing. The atoms on the surface of the sample inelastically scatter a small percentage of the incident electrons. Some of the “reflected” electrons satisfy the Bragg condition, leading to the formation of high-angle Kikuchi pattern dependent upon the crystallographic planes on which they were incident. The subsequent pattern captured on a fluorescent screen is composed of characteristic lines termed the

Kikuchi bands. The patterns composed of lines are rapidly processed using the Hough transform into points in Hough space. The orientation of the crystal lattice, with respect to the sample coordinate system, at the incident point is subsequently extracted [6].

Researchers have made use of X-ray diffraction analysis to determine the crystalline structure of the weld metal [7]. Analysis showed that the columnar grains solidify along the [100] crystal axis, with the austenite taking the face centred cubic (FCC) unit crystal. Hence the researchers subsequently used macrographs to identify several distinct homogeneous regions where the dendrites had uniform grain orientation [7].

In the DISSIMILAR project the crystallographic orientation of the entire weld cross-section at several positions is mapped using EBSD. Figure 5 shows a macrograph of a dissimilar weld composed of similar material to the weld shown in Figure 1. The weld was sectioned into 7 zones for scanning by EBSD; this paper will make use of the weld structure in zone 1, the weld root.

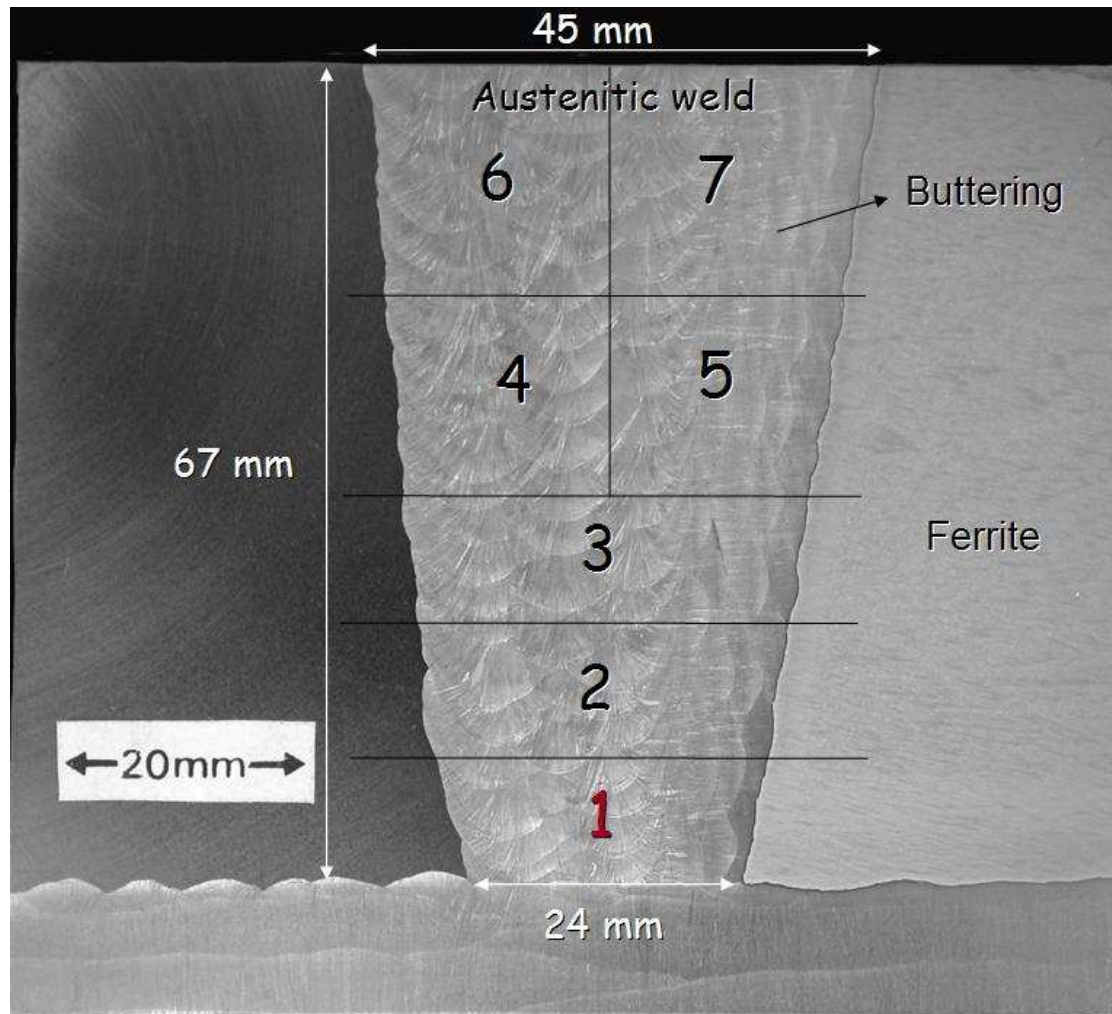


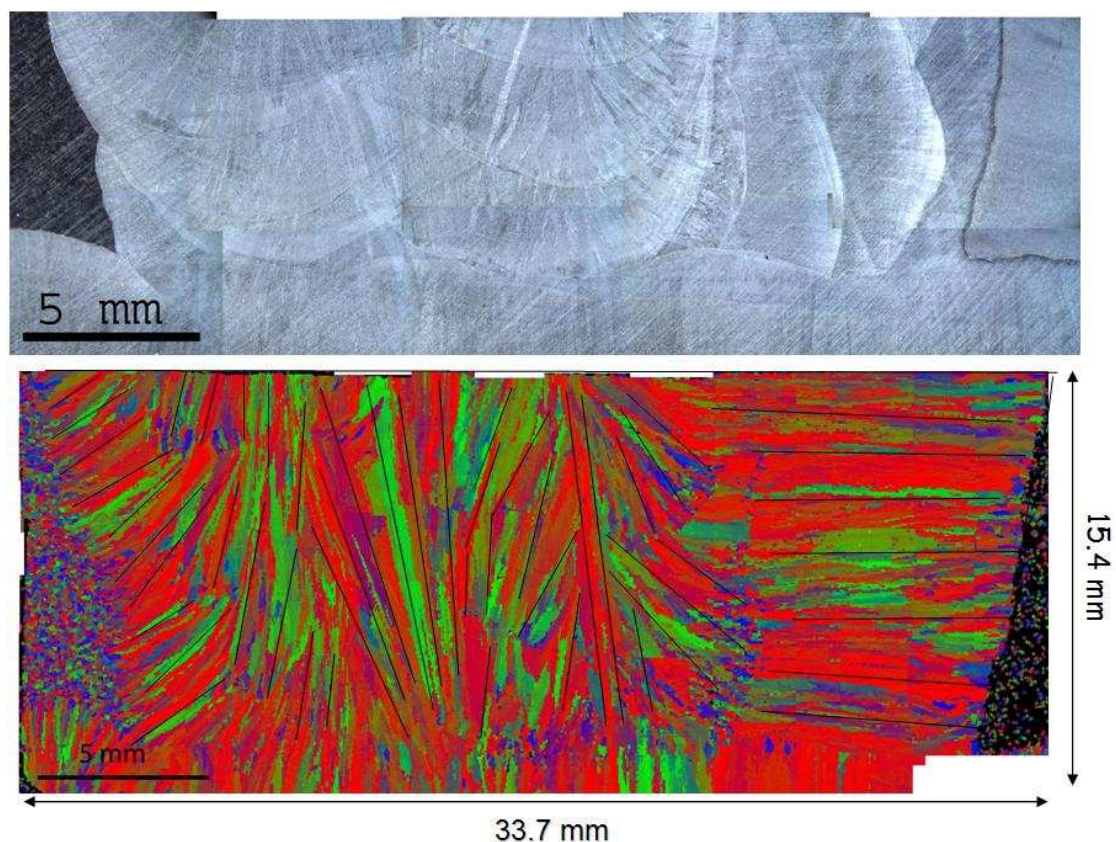
**Figure 5** An austenitic weld showing the buttering and cladding layers, and the section zones for EBSD scanning.

For scanning the weld map cost effectively through EBSD the spatial scanning resolution must be established. The scanning resolution impacts on the time taken to generate the map: scan of an area  $\sim 4\text{mm}^2$  at a resolution of  $5\mu\text{m}$  takes  $\sim 6$  hours whereas the same area at a resolution of  $40\mu\text{m}$  takes only 6 minutes. The transducer frequency was set at 2MHz generating a longitudinal wave with a wavelength of  $\sim 3\text{mm}$ . Assuming the dominant Rayleigh scattering mechanism [1] the wave would be sensitive to a minimum scatterer size of  $300\mu\text{m}$ , ie  $1/10$  of the wavelength. Hence a scanning resolution of  $40\mu\text{m}$  was deemed sufficient to capture significant regions within the weld.

The second important parameter to establish is termed the misorientation angle. The EBSD data is represented as a colour map where each colour corresponds to a particular orientation of the crystal structure with regard to the sample coordinate system. The orientation of the crystals can be

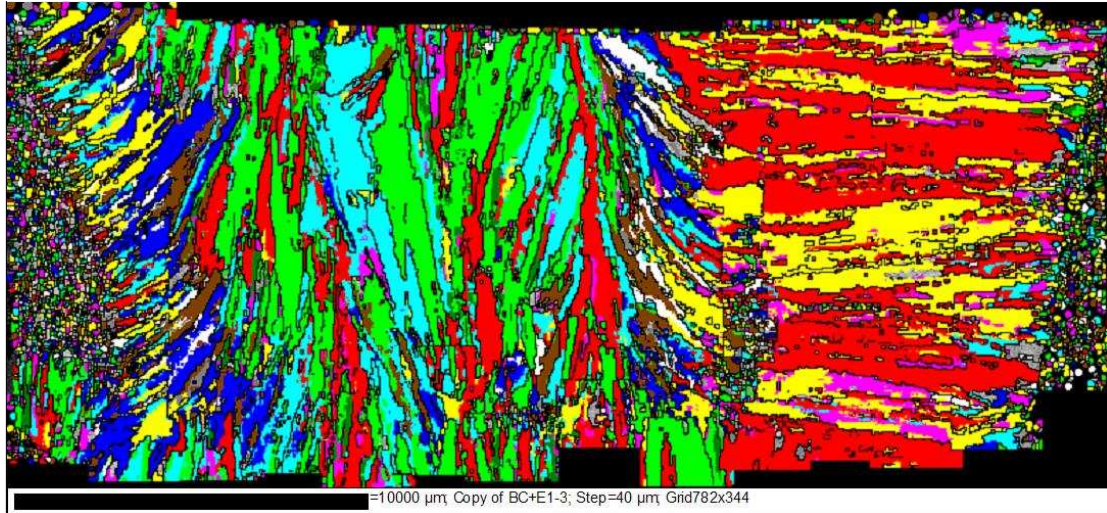
expressed in terms of the three Euler angles [6] which are rotations performed in a specific sequence to transform the sample coordinate system onto the crystal coordinate system. The misorientation parameter is used to define the position of the grain boundaries, ie the higher the parameter the smaller the numbers of grain boundaries. Establishment of this parameter is an ongoing activity in the DISSIMILAR project and is subject to modification due to both experimental validation results and parametric modelling studies of significant orientation mismatches across boundaries. On the first iteration, the misorientation parameter was again set using the Rayleigh scattering assumption, ie the misorientation angle is that which leads to the size of the regions in the path of the propagating wave being no less than  $300\mu\text{m}$ , the minimum scatterer size. An advantage of the misorientation parameter, unlike the scanning resolution, is that any value can be chosen post-scanning, as it is applied on the collected data to generate the maps.

Figure 6 shows the macrograph of zone 1 and the associated EBSD map, where faint black lines within the scan map illustrate general orientation of homogeneous regions. Firstly, note the impact of different deposition procedures for the weld and the buttering, where the buttering was applied prior to flat 1G position manual deposition of the weld. Secondly, the grains appear to grow through several deposit runs leading to the characteristic columnar grain structure observed in austenitic welds.



**Figure 6** The macrograph of zone 1 and the associated EBSD orientation map; scanned at a resolution of  $40\mu\text{m}$  and processed with a misorientation parameter of  $20^\circ$ .

The weld map, however, had excessive boundaries for cost effective expression within models. Hence a processing method was devised termed 'orientation unification'. In this technique several dominant orientations are identified within the weld map shown in Figure 6. Subsequently, an angular spread of between  $15$  and  $20^\circ$  either side of the dominant orientation is set to be equal to the dominant orientation; all other regions (and those smaller than the minimum scatterer size) take the nominal orientation of the grain or that of the parent. In addition, the Euler angles (referenced to the axes of the unit cubic cell) are transformed to the rotation angles following the rotation sequence adapted by the simulation program. Figure 7 shows the processed weld map ready for input to the ultrasonic models and Table 1 shows the ten selected dominant orientations for zone 1. The development of the orientation unification technique is ongoing in the DISSIMILAR project and is subject to feedback from experimental validation trials.



**Figure 7** Processed weld map for input to the models; the ten dominant orientation regions are detailed in Table 1.

**Table 1** The ten dominant orientations selected for the weld map of zone 1; the crystallographic orientations are expressed as three rotation angles about the x, y and z axes of the component reference frame, as required for ultrasonic modelling.

Colour	$\alpha(^{\circ})$ (rotation about x)	$\beta(^{\circ})$ (rotation about y)	$\gamma(^{\circ})$ (rotation about z)
<b>Red</b>	0	0	0
<b>Blue</b>	0	0	45
<b>Lime green</b>	318.72	6.37	193.09
<b>Yellow</b>	12.55	28.25	18.91
<b>Cyan</b>	8.17	4.52	338.91
<b>Brown</b>	30.81	-13.14	29.96
<b>Pink</b>	348.11	-22.77	177.97
<b>Green</b>	21.73	-1.78	8.36
White	351.5	-22.86	138.12
<b>Black</b>	19.95	-1.16	56.60

The elastic stiffness of the various mapped regions of the weld has to be determined to model the propagation of a stress (ie sound) wave. In a previously reported approach [7], a thin sample from a region of the weld containing columnar grains oriented in the same direction was removed. The stiffness was then evaluated using through-transmission experimental measurement of ultrasonic velocities. The weld was then discretised into regions where the grains had similar orientations, the assumption being that the solidification direction along the [100] axis is in the orthogonal plane to the welding direction, and that all the homogenized regions of the weld contain similar columnar grains such that the weld can be described using just the angle of the columnar grain orientation [7].

Figure 7 shows that the weld and buttering consist of grains of differing crystallographic makeup, hence the EBSD map offers the possibility to describe the weld in its full three-dimensional state. In the DISSIMILAR project the stiffness is evaluated using a single-crystal of the weld alloy grown through a casting process. The velocity of the longitudinal and the two polarized shear waves along [100], [110] or the [111] are related, by Newton's law of motion, to the stiffness of the cubic crystal. The results presented in this paper make use of the cubic stiffness constants measured on an alloy of similar composition to the weld presented in Figure 5 using velocity measurements in a single-crystal [8]. The measured stiffness constants are  $C_{11}=203.6\text{GPa}$ ,  $C_{12}=133.5\text{GPa}$  and  $C_{44}=129.8\text{GPa}$ .

## Modelling

Modelling the propagation of an elastic stress wave through an anisotropic medium has been incorporated into the CIVA modelling suite developed in the French nuclear agency Commissariat à l'Énergie Atomique (CEA) [9]. The CIVA model is being used within TWI for a wide variety of tasks, including the optimisation of probe parameters, technical justifications and design of inspection procedures. TWI has undertaken an extensive validation programme of the various models within the platform and this effort is ongoing. Additionally, a large body of work in various organisations around the world continues to build confidence in the capabilities of the suite of models available in CIVA.

In the DISSIMILAR project the CIVA model is being used as the primary platform to develop, test and optimise the strategies to overcome the distortion of the austenitic weld. The semi-analytical codes to model ultrasonic wave propagation and interactions with discontinuities in anisotropic media are cost effective for industrial parametric studies, in comparison to finite element/difference codes which are computational and time intensive.

A recent example of the current capabilities of CIVA to deal with anisotropic media was illustrated through the ultrasonic inspection of a 69mm thick K-prep 316L austenitic weld [10]. The inspection of the weld with a 2MHz single element transducer generating a 60° longitudinal wave was both simulated and experimentally evaluated on a mockup specimen. The distortion of the propagating sound beam was simulated by the CIVA model and compared to experimental results [10]. In general, the experimental evidence was consistent with the model predictions; however there were discrepancies in signal amplitudes and echodynamics. This shows the importance of describing the weld structure accurately, as well as the need for validation of the model. The authors conclude with the importance of taking into account the distortion to better design the inspection and improve sizing of defects [10].

In the DISSIMILAR project, the weld map of Figure 7 was processed using a digitizer to generate a 2D CAD drawing. The boundaries were manually identified according to the criteria of minimum scattering regions/distances. Figure 8 shows the expression of the zone 1 weld cross-section within the CIVA model, containing 89 closed regions leading to a total of 1276 boundaries. The weld cross-section is extruded to create the three dimensional component, ie assumes that the weld structure is uniform along the welding direction.

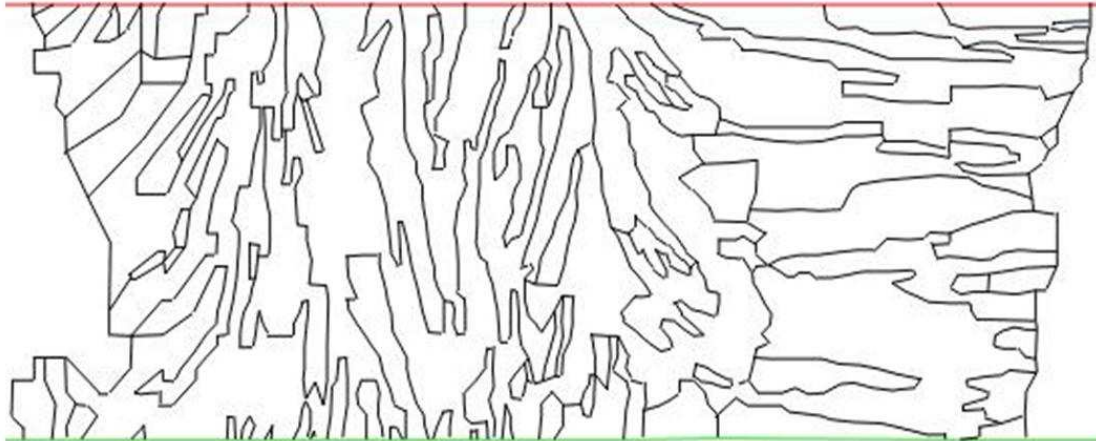


**Figure 8** The CAD drawing of the zone 1 weld cross-section input into the CIVA model. The drawing consists of 89 closed regions with a total of 1276 boundaries.

The CIVA model is used here to illustrate the distortion induced by the microstructure onto the sound field. In all the results presented in this paper a 2MHz linear phased array probe with a pitch of 1.5mm is used in the inspection simulations. Figure 9(a) shows the ray trace of a 16 element array generating a 45° longitudinal wave beam (green trace) and associated shear beam (red trace) within zone 1 of the weld, when all the regions in the weld take the stiffness value of the parent austenitic, ie the weld is isotropic. Note that the array is not programmed to focus the sound field, only steer. Figure 9(b) shows the ray tracing of the sound beams when the full anisotropic weld structure is input, ie each region takes the set dominant orientations. The distortion due to the microstructure is illustrated by the ray tracings which are no longer straight; note that the red shear wave of Figure 9(a) becomes two orthogonally polarized shear wave components in the three-dimensional anisotropy of the weld in Figure 9(b).

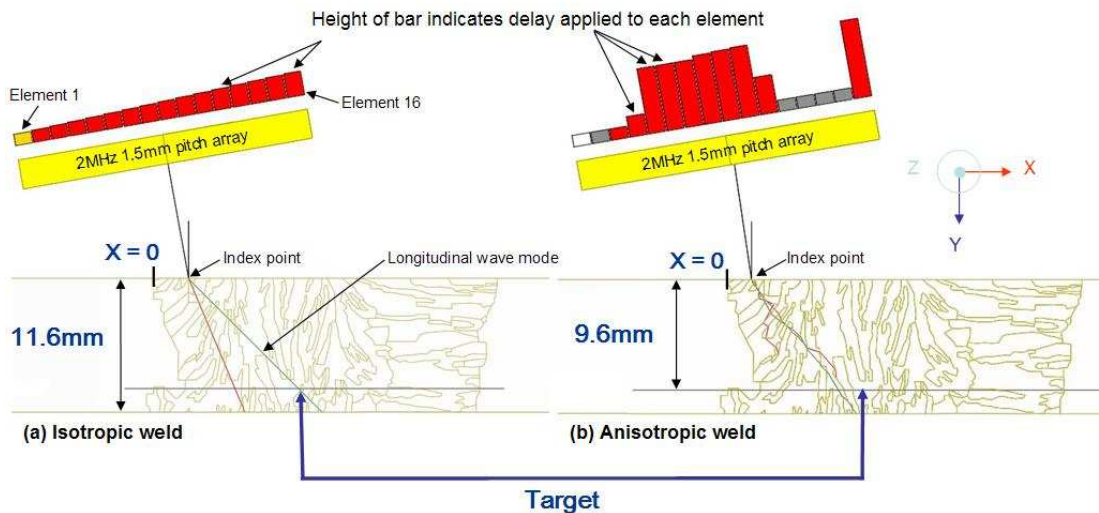


**Figure 9** Ray tracing of a 2MHz 16 element array with a pitch of 1.5mm programmed to generate a 45° beam within (a) an isotropic weld and (b) anisotropic weld measured by EBSD. The array was inclined at 10° to the horizontal and is in immersion with a water path of 10mm.

The bars above the array associated with each element represent the delay applied to each element. The delay law applied for the isotropic weld in Figure 9(a) dictates that the first element fires first followed by successive firing of the adjacent element up to element number 16. Hence the delay of elements 2 to 16 are relative to element 1 which fires at time equals zero. In Figure 9(b) the CIVA model has used the criteria of generating a longitudinal beam at 45° to set the delay law such that only those elements which contribute to the goal are activated, ie elements 1, 2, 12, 13, 14 and 15 are turned off. Note, however, the microstructural condition does not appear to allow optimisation of the delay law such that the longitudinal ray trace passes through the same target point as in the isotropic medium.

The beam sections in the x-z plane 9.6mm from the surface (see Figure 9) are evaluated using the CIVA model; Figure 10 shows the results of the three cases which were considered. Note that the index point of the sound incident on the surface of the component was at  $x=3\text{mm}$  (see Figure 9). Figure 10(a) presents the beam of the case shown in Figure 9(a), ie the weld is isotropic and the beam is generated using the isotropic delay law, and the beam profile is as expected. Figure 10(b) represents the case shown in Figure 9(b), ie with the anisotropic weld properties included and the delay law calculated by CIVA to propagate the beam. The distortion due to the microstructure is revealed by the output and the maximum amplitude of the beam in Figure 10(b) is 27dB less than the isotropic case shown in Figure 10(a).

A further case was considered, shown in Figure 10(c), where the isotropic delay law shown in Figure 9(a) was used to generate the sound and propagate it within the anisotropic weld. The loss in signal amplitude in the case shown in Figure 10(c) was only 19dB less than the isotropic case. Hence, turning off elements in the array when generating the delay law (ie the anisotropic delay law generated by CIVA for the case shown in Figure 10(b)) reduces the amount of energy coupled into the weld, which would in turn impact on the S/N performance of the inspection.

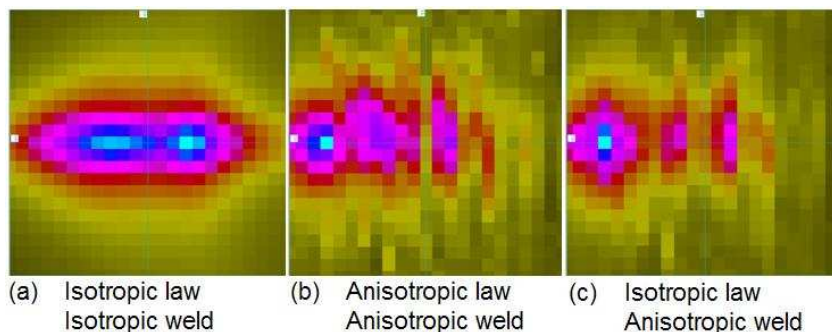


**Figure 10** Beam sections calculated in the x-z plane at depth of 9.6mm from surface for (a) isotropic delay law for an isotropic weld, (b) anisotropic delay law calculated by CIVA for an anisotropic weld and (c) the isotropic delay law applied for an anisotropic weld.

A simulation of using the 2MHz 16 element probe to scan the weld along a line from  $x=-5\text{mm}$  to  $x=9\text{mm}$  with a resolution of 1mm was performed. A 3mm diameter side drilled hole (SDH) target was introduced at a depth of 9.6mm, ie where the beam sections of Figure 10 were evaluated. Figure 11 shows the results of the simulated scan.

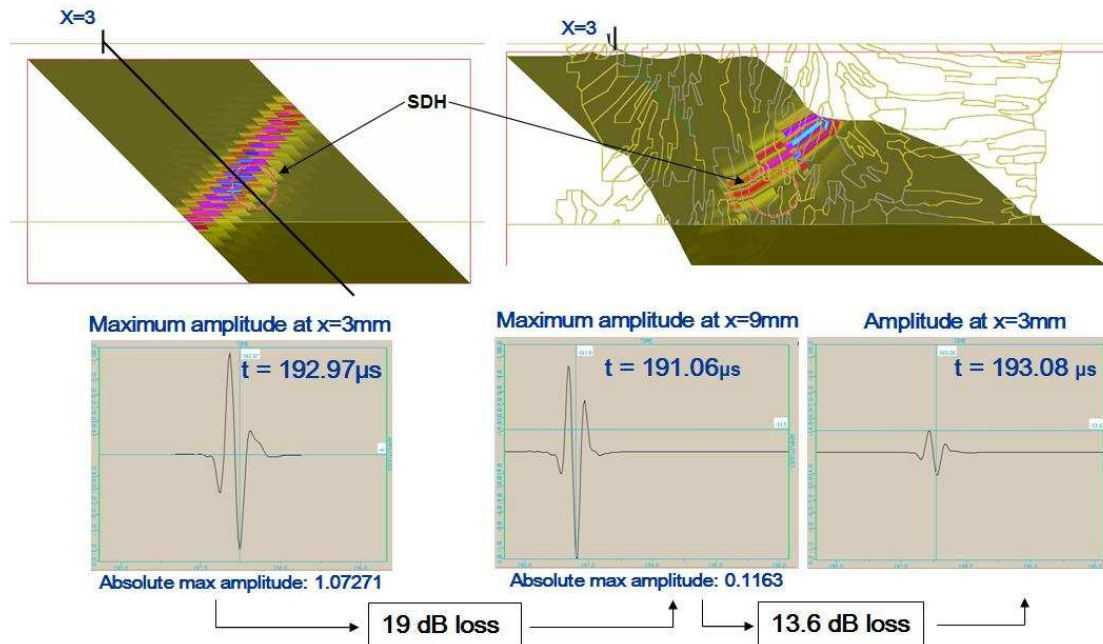


**Figure 11** A simulated scan in CIVA from an index point of  $x=-5\text{mm}$  to  $x=9\text{mm}$ . A 3mm SDH was introduced at a depth of 9.6mm from the surface in an isotropic medium (left) and in the anisotropic weld (right).

In the isotropic case of Figure 11, the  $45^\circ$  beam is directly incident on the SDH at an index position of  $x=3\text{mm}$  giving the largest signal amplitude. However, in the anisotropic case the maximum signal amplitude was received at an index position of  $x=9\text{mm}$ , which is 19dB below the signal received from the target SDH in the isotropic case (see Figure 11). In fact, at  $x=3\text{mm}$  in the anisotropic case shown in Figure 11, the signal strength was 13.6dB weaker than at  $x=9\text{mm}$  in the same case. Note that the model only resolves the interaction of the sound field with the SDH target, ie no boundary interactions are evaluated, such that no back scattered noise signals are predicted.

In summary, the observed errors in plotting signals from flaws due to the distortion of the sound field by the microstructure of austenitic welds is predicted by the CIVA simulation platform. In the ongoing DISSIMILAR project, the predictions of the CIVA model will be validated with experimental data and the effectiveness of the EBSD route to quantify the microstructure will be assessed. The main aim of the project, however, is the development of strategies to overcome the distortion induced by the microstructure.

## STRATEGIES

### Adapted focal laws to maximise sensitivity

As noted in Figure 10, reducing the number of elements used on an array directly impacts on the energy coupled into the weld, subsequently reducing the sensitivity of the inspection. Hence the delay law should aim to make use of all available elements on the array. The anisotropic microstructure of the weld induces different travel paths to waves emanating from different position on the surface. This is illustrated by the simulated arrival times of the signals due to the SDH in Figure 11. In the isotropic case (shown on the left of Figure 11) the arrival time of the peak signal due to the SDH was  $192.97\mu\text{s}$  at a probe index position of  $x=3\text{mm}$ , whereas within the anisotropic weld (shown on the right) at a probe position of  $x=3\text{mm}$  the signal was received at  $193.08\mu\text{s}$ ,  $0.11\mu\text{s}$  later. This implies that the actual travel path to the SDH target in the anisotropic weld is longer than a straight line path.

The proposed strategy to improve sensitivity makes use of all available elements on the array to generate focal laws ‘adapted’ to the anisotropic condition of the weld. The widely divergent sound field generated by each element on the array will be distorted by the microstructure but some of the energy will be incident on the target area. The fundamental theory underlying the algorithms of focal law calculators to focus the sound energy from an array is to ensure that the wave fronts from each element arrive at the target position at the same time and in the correct phase to constructively generate a maximum in sound pressure. The adapted focal laws will be generated by using simulations to predict the actual time at which the sound energy from all the elements arrives at the required target region.

The concept is illustrated using zone 1 of the weld (shown in Figure 5), its anisotropy quantified by EBSD (see Figure 7) and expressed within the CIVA simulation platform. A 2MHz linear array with 8 elements at a pitch of 1.5mm is coupled to the model description of zone 1 of the weld in immersion testing. The probe was inclined at an angle of 10° to the horizontal and the index point of the probe was set to x=2mm (see Figure 12). In the case presented in this paper, a water path length of 140mm is selected to place the SDH target very close to the range of the natural near field point (end of the Fresnel zone) of the array.

The simulation shown in Figure 12 is used to first illustrate that the concept of generating the delay law through received signals from the target SDH (ie the adapted law) is sound, since at the near field range its performance should be similar to that of the calculated law. Secondly, the simulation is used to study the sensitivity of the received signal amplitude in two different scenarios: (1) the null-point of the wave, where the arrival phase of all waves is at zero amplitude, was chosen as the reference to generate the adapted delay law, and (2) the adapted law generated was reversed without taking into account the pulse-echo nature of the travel time. Both these scenarios illustrate the degree of S/N performance change that could take place due to the nature of the delay law used when inspecting an anisotropic weld, as well as the precision available in the simulation platform.

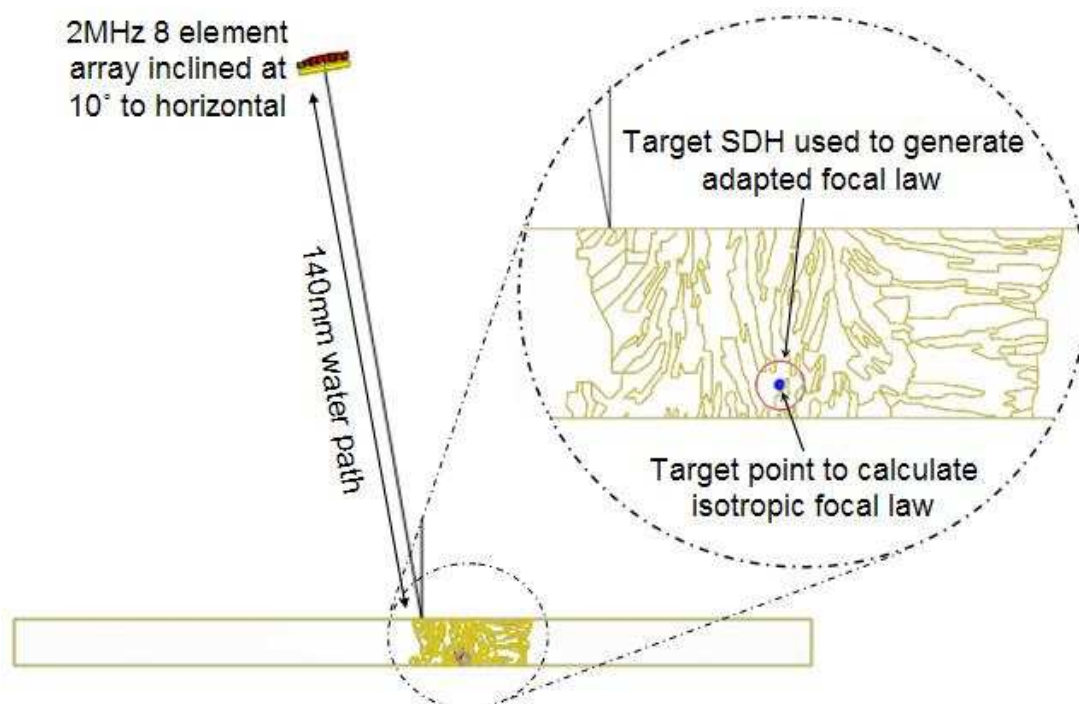


**Figure 12** Simulation of the anisotropic weld inspection with a 2MHz linear array of 8 elements at a pitch of 1.5mm, inclined at 10° to the horizontal with a water path of 140mm; the index point of the probe was set to x=2mm.

The isotropic delay law was calculated by ensuring that the sound energy from all 8 elements arrives at the target point (see Figure 12) at the same time and in phase to constructively interfere for maximum sound pressure; the algorithm used was termed ‘single point focusing’ in the CIVA model. The adapted focal laws were not calculated mathematically. Each element of the array was fired and received on, generating a reflected signal from the target SDH shown in Figure 12, while all other elements were turned off. Each element, due to its small size, would generate a widely divergent beam and the model evaluates the interaction of this beam front with the SDH after traversing the anisotropic

weld. Due to the distortion induced by the microstructure, sound energy emanating from different points (ie elements) on the array will take different paths to the SDH. This is shown in the A-scan signals from the SDH due to the 8 elements where the arrival times are offset with respect to each other, as shown in Figure 13, and the non-uniformity of the offsets suggests that it is induced by a phenomenon in addition to the difference in the geometrical direct line paths to the target SDH. Figure 13 also shows the difference in received signal amplitude with respect to that of element 1, illustrating the degree to which the microstructure influences the propagation of sound energy within the weld.

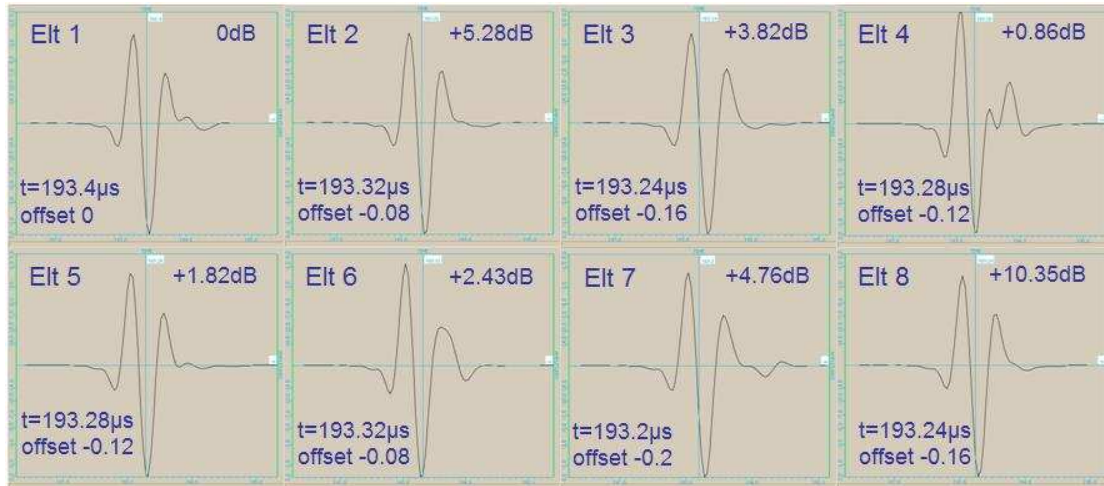


**Figure 13** A-scans from each of the 8 elements collected independently of all others. The arrival times are shown, with their offset from element 1, along with the change in received amplitude relative to element 1.

The simulated arrival times to the target are used to generate the adapted focal law, following the same criteria as for the calculated focal law (assuming an isotropic weld): the wave fronts must arrive at the target at the same time and in phase to maximise the sound energy. The isotropic and adapted focal laws applied to the 8 element array are illustrated in Figures 14(a) and 14(b) respectively, along with the resultant echo signal from the SDH target. In addition, the results from the two scenarios described earlier are shown in Figure 14(c) and 14(d).

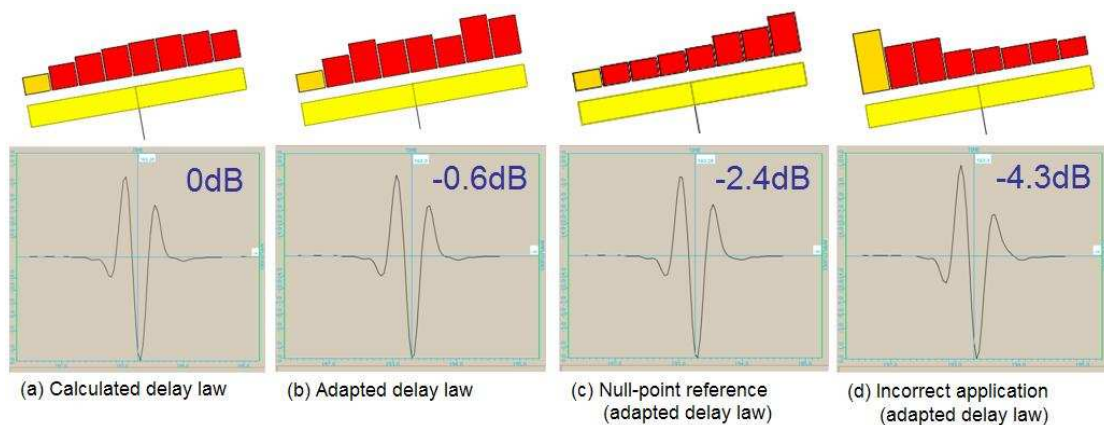


**Figure 14** Illustration of (a) calculated focal law assuming isotropic conditions, (b) adapted focal laws generated through simulation, (c) adapted focal law generation using the null-point of the received signal as reference and (d) incorrect adapted delay law, applied in reverse to the array without accounting for pulse-echo travel path.

The adapted law (Figure 14(b)) showed similar performance to the calculated law (less than 1dB) at the near field range, which is at the edge of the range at which the delay laws begin to impact on the S/N performance. The sensitivity of the received signal to changes in the applied delay laws of less than  $0.1\mu\text{s}$  (shown in Figures 14(c) and 14(d)) illustrate the level of change in S/N performance

that could be observed even at the edge of the applicable envelope (ie the near field range). Hence the concept of adapting the focal laws to the microstructure of the weld could lead to significant improvement in S/N performance. However, in this paper, the concept has been illustrated using a static probe (ie not scanning) and the concept (hence the model) will also be experimentally validated in the DISSIMILAR project. In particular, the question of how the adapted focal law performs in regions to which it was not optimised must be investigated, along with how the back scattered grain noise behaves; these aspects will be investigated primarily through an experimental programme.

The use of finite element codes modelling the full EBSD weld map at a resolution of  $40\mu\text{m}$  is also being investigated in the DISSIMILAR project for generating the adapted focal laws, ie as an 'adapted delay law calculator for anisotropic media'. Finite elements codes currently take excessive computing resources and time to simulate full ultrasonic inspections, which can be done more cost effectively, in relative terms, by the semi-analytical codes employed in the CIVA simulation platform. However, greater precision in the delay law curves could be achieved through the use of the finite element codes which model the full anisotropy of the weld without simplifications, ie splitting the weld map into regions of dominant orientation for input into the CIVA model.

### Translation tables to correct for positional errors

The second of the proposed strategies would be implemented post-scanning to correct the plotting positions of indications. To implement the concept 'translation tables' will be generated for the weld using simulations in the anisotropic weld. For each probe position, each beam angle and each target (represented by a SDH) within the weld, a simulation is run. The results would show the shift in positions of each target within the weld in comparison to its actual position. The shift is then noted in a set of tables as shown in Figure 15. The tables are then used during the actual inspection to determine the possible positions of any detected indications depending on the beam angle ( $\theta$ ) and position of the probe ( $d$ ).

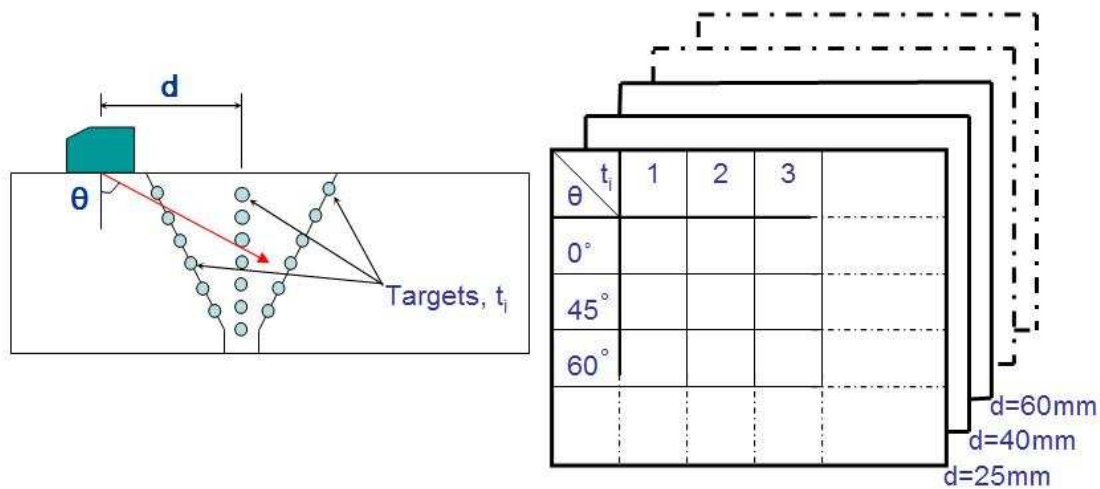


**Figure 15** Generation of the translation tables through the simulation of the inspection for different beam angles, probe positions and target positions.

In the DISSIMILAR project the generation of the translation tables through simulations will be recreated by experimental measurements. Several weld sections will be taken and, in each section, several SDH targets will be introduced. The positional errors in the plotting of the signals generated by these targets (for different beam angles and probe positions) will be compared to the predicted ones. Comparison of the experimental and the simulated data will aid in the validation of the model and an assessment of the method used to quantify the microstructure.

### Issues

The EBSD technique is only being used to evaluate the crystalline orientation of the weld on the transverse plane to the welding direction. A non-destructive experimental method has been devised in the DISSIMILAR project to evaluate the microstructural uniformity of the weld along the welding

direction. In addition, full EBSD maps of the weld at several positions along it are being generated to quantify the degree to which the microstructure changes along the welding direction.

As stated earlier, the scanning resolution for generating the EBSD maps determine how long each scan takes. At the 40 $\mu$ m resolution used for the scan of zone 1 shown in Figure 5 the total time for scanning alone is estimated at about 10 hours, excluding the considerable amount of time for sample preparation. To prepare, scan and process several full weld cross-sections in the DISSIMILAR project the total time is measured in weeks. Hence this method is costly and is only likely applicable for critical welds, where the consequences of failure would be economically, environmentally and socially catastrophic. Future developments in EBSD technology could lead to a reduction in the times taken to generate the weld maps, opening the possibility of application to a wider set of components.

Similar to EBSD scanning, the time taken to simulate a single case with an anisotropic weld in comparison to an isotropic case on the CIVA platform is considerable. For example, the time taken to run the case in the isotropic weld shown in Figure 10(a) was 1 minute, whereas it took 7.5 hours to compute each of the other two cases in the anisotropic weld. Similarly, the isotropic case shown in Figure 11 was completed in 4 minutes while the anisotropic case took in excess of 100 hours.

Clearly this has implications towards the applicability of the proposed correction strategies as even larger weld maps (compared to the zone 1 presented in this paper) need to be modelled, as well as more complex probe designs with up to 128 elements. Furthermore, to generate the translation tables a vast number of simulations need to be run. A proposed simplification is to model the anisotropy in the path of the propagating wave, while assigning isotropic properties to the remaining regions of the weld. Modelling times could be reduced by coding faster numerical stencils or modifying parameters. The most practical route available presently is to increase as much as possible the computing resources available to run the model.

Empirical modelling studies of the significant orientation changes across a boundary (ie grain boundary) are underway in the DISSIMILAR project in order to identify and limit the number of different dominant orientation regions. Similarly investigations into the effect of compositional variation on the elastic stiffness of alloy single-crystals in comparison to the stiffness of the dominant element are being undertaken.

An important aspect of the work has to be validation, as noted by other researchers in the field [10]. The use of models, especially for critical applications, has to be subject to stringent evidence, not only to qualify their applicability but, more importantly, to establish the limits to their validity.

## CONCLUSIONS

The following conclusions are drawn from the work done to date in the ongoing DISSIMILAR project:

1. The evidence to date shows that the application of the strategy to better design the focal laws by taking into account the anisotropic microstructure has potential to improve inspection quality. In the project this strategy is being tested and validated using a specimen with implanted flaws. The proposed use of translation table is novel and the concept is also being developed in the project.
2. A technique termed orientation unification has been devised to translate the orientation map generated by EBSD into the ultrasonic simulation platform. The technique is being refined and optimised to set the dominant orientations in order to reduce the number of regions required to describe the weld.
3. The methods being explored are only applicable to welds in critical components (such as the safe-end weld in a reactor pressure vessel) due to the cost, complexity and time required for implementation.
4. For the proposed solutions to the inspection of austenitic welds to be accepted by industry, the simulation results will be validated.

## ACKNOWLEDGEMENTS

The authors would like to thank all members of the DISSIMILAR consortium (British Energy, Shell UK, HSE Nuclear Installations Inspectorate, Peak NDT, ALBA Ultrasound, Applied Inspection, Birmingham University and TWI) for their support and encouragement.

The DISSIMILAR project is part funded by the United Kingdom's Technology Strategy Board.

## REFERENCES

- 1) Krautkrämer J and Krautkrämer H, *Ultrasonic testing of materials*, New York, Springer-Verlag, 1990.
- 2) Nageswaran C, Bird C and Whittle A C, "Immersion transmit-receive longitudinal phased array probe for stainless steel", *Insight*, December 2008, Vol 50(12), 673-684.
- 3) Anderson M T, Crawford S L, Cumblidge S E, Diaz A A and Doctor S R, "Low frequency phased array methods for crack detection in cast austenitic piping components", *6<sup>th</sup> Int. Conf on NDE in Relation to Structural Integrity for Nuclear and Pressurised Components*, Budapest, 2007.
- 4) Lozev M, Patel P and Spencer R, "Optimization and validation of phased-array ultrasonic techniques for inspection of clad piping dissimilar materials welds", *6<sup>th</sup> Int. Conf on NDE in Relation to Structural Integrity for Nuclear and Pressurised Components*, Budapest, 2007.
- 5) Nageswaran C and Bird C, "Evaluation of the phased array transmit-receive longitudinal and time-of-flight diffraction techniques for inspection of a dissimilar weld", *Insight*, December 2008, Vol 50(12), 678-684.
- 6) Randle, V., "Microtexture determination and its applications", London, Institute of Materials, 1992.
- 7) Dupond O, Chassignole B, Doudet L and Birac C, "Methodology for modelling ultrasonic inspection of an austenitic stainless steel weld", *6<sup>th</sup> Int. Conf on NDE in Relation to Structural Integrity for Nuclear and Pressurised Components*, Budapest, 2007.
- 8) Lenkkeri J and Juva A, "The effect of anisotropy on the propagation of ultrasonic waves in austenitic stainless steel", *Reliability of Ultrasonic Inspection of Austenitic Materials*, Belgium, 1980.
- 9) Mahaut S, Chatillon S, Leymarie N, Jenson F and Calmon P, "Simulation tools for predicting non destructive testing of heterogeneous and anisotropic structures", *Int. Conf on Ultrasonics*, Vienna, 2007.
- 10) Chassignole B, Paris O and Abittan E, "Ultrasonic examination of a CVCS weld", *6<sup>th</sup> Int. Conf on NDE in Relation to Structural Integrity for Nuclear and Pressurised Components*, Budapest, 2007.